

form them. Global 3D models of binary systems and detailed global MHD disk simulations are two problems of immediate interest. The other approach is a more detailed simulation of a small local region within a disk that includes more complex physics. Examples include radiation transport, partial ionization, buoyancy, reconnection, and improved equations of state. Both of these tasks require significant computer resources. Both kinds of simulation have led, and will lead, to significant progress in furthering our understanding of accretion disks. Larger simulations with greater resolution can take advantage of the latest advances in computer speed, but including more physics in the model will depend as much on new algorithms and insightful analysis as on new hardware.

A crucial recent development has been the discovery that a local MHD instability produces precisely the type of turbulence necessary to transport angular momentum outward within the disk. We are now in the position to address specific questions of accretion disk dynamics from first principles. For example, we can study precisely what sort of transport levels are to be found in disks (or in the usual parlance, the value of α) and whether the instability can act as a dynamo and amplify magnetic fields. Magnetic buoyancy and reconnection are two important physical processes limiting magnetic field strength that require further attention. Of course, the relevant equations are by no means simple; understanding accretion disks has become, in large part, the task of understanding 3D, nonisotropic, radiative, inhomogeneous MHD turbulence. Considering the effort that has gone into investigating hydrodynamic turbulence in much simpler contexts, the problems are daunting. But prospects are far from bleak. The recent strides in understanding turbulence made possible by numerical simulations (36) hold forth the promise of similar advances in accretion disk modeling.

REFERENCES AND NOTES

1. A. L. Kinney, in *The First Stromlo Symposium: The Physics of Active Galaxies*, G. V. Bicknell, M. A. Dopita, P. J. Quinn, Eds. (Astronomical Society of the Pacific, San Francisco, CA, 1994), pp. 61–71.
2. D. Lynden-Bell, *Phys. Scr.* **17**, 185 (1978).
3. M. Herant, W. Benz, W. R. Hix, C. L. Fryer, S. A. Colgate, *Astrophys. J.* **435**, 339 (1994).
4. N. I. Shakura and R. A. Sunyaev, *Astron. Astrophys.* **24**, 337 (1973).
5. K. Home, *ibid.* **297**, 273 (1995); in *Theory of Accretion Disks-2*, W. J. Duschl et al., Eds. (Kluwer Academic, Dordrecht, Netherlands, 1994), pp. 77–91.
6. L. L. Smarr, *Science* **228**, 403 (1985).
7. D. N. C. Lin and J. C. B. Papaloizou, *Mon. Not. R. Astron. Soc.* **191**, 37 (1980).
8. D. Ryu and J. Goodman, *Astrophys. J.* **388**, 438 (1992).
9. W. Cabot and J. B. Pollack, *Geophys. Astrophys. Fluid Dyn.* **64**, 97 (1992); W. Kley, J. C. B. Papaloizou, D. N. C. Lin, *Astrophys. J.* **416**, 679 (1993); J. M. Stone and S. A. Balbus, in preparation.

10. J. C. B. Papaloizou and J. E. Pringle, *Mon. Not. R. Astron. Soc.* **208**, 721 (1984).
11. P. Goldreich, J. Goodman, R. Narayan, *ibid.* **221**, 339 (1986).
12. J. F. Hawley, *ibid.* **225**, 677 (1987).
13. J. Goodman, R. Narayan, P. Goldreich, *ibid.*, p. 695.
14. O. M. Blaes and J. F. Hawley, *Astrophys. J.* **326**, 277 (1988).
15. J. F. Hawley, *ibid.* **381**, 496 (1991).
16. O. M. Blaes, *Mon. Not. R. Astron. Soc.* **227**, 975 (1987).
17. M. Różyczka and H. C. Spruit, *Astrophys. J.* **417**, 677 (1993); *ibid.*, videotape, segment 3.
18. K. Sawada, T. Matsuda, I. Huchisa, *Mon. Not. R. Astron. Soc.* **219**, 75 (1986).
19. H. Spruit, *Astron. Astrophys.* **184**, 173 (1987).
20. R. Whitehurst, *Mon. Not. R. Astron. Soc.* **232**, 35 (1988); M. Hirose and Y. Osaki, *Publ. Astron. Soc. Jpn.* **42**, 135 (1990); S. Lubow, *Astrophys. J.* **381**, 268 (1991); R. Whitehurst, *Mon. Not. R. Astron. Soc.* **266**, 35 (1994).
21. J. Goodman, *Astrophys. J.* **406**, 596 (1993).
22. S. H. Lubow, J. E. Pringle, R. R. Kerswell, *ibid.* **419**, 758 (1993).
23. D. Ryu and J. Goodman, *ibid.* **422**, 269 (1994).
24. Ya. B. Zel'dovich, A. A. Ruzmaikin, D. D. Sokoloff, *Magnetic Fields in Astrophysics* (Gordon and Breach, New York, 1983), p. 321.
25. S. A. Balbus and J. F. Hawley, *Astrophys. J.* **376**, 214 (1991).
26. E. P. Velikhov, *Zh. Eksp. Teor. Fiz.* **36**, 1398 (1959).

- The stability criterion was extended to general rotation laws for Couette cylinders by S. Chandrasekhar [see his classic text *Hydrodynamic and Hydromagnetic Stability* (Oxford Univ. Press, London, 1961)].
27. J. F. Hawley and S. A. Balbus, *Astrophys. J.* **376**, 223 (1991).
 28. S. A. Balbus, *ibid.*, in press.
 29. K. Shibata and Y. Uchida, *Publ. Astron. Soc. Jpn.* **38**, 631 (1986).
 30. J. M. Stone and M. L. Norman, *Astrophys. J.* **433**, 746 (1994).
 31. ———, *Astrophys. J. Suppl. Ser.* **80**, 791 (1992).
 32. J. F. Hawley and S. A. Balbus, *Astrophys. J.* **400**, 595 (1992).
 33. J. Goodman and G. Xu, *ibid.* **432**, 213 (1994).
 34. J. F. Hawley, C. F. Gammie, S. A. Balbus, *ibid.* **440**, 742 (1995).
 35. A. Brandenburg, Å. Nordlund, R. F. Stein, U. Torkelsson, *ibid.* **446**, 741 (1995); J. M. Stone, J. F. Hawley, C. Gammie, S. A. Balbus, in preparation.
 36. N. Brummell, F. Cattaneo, J. Toomre, *Science* **269**, 1370 (1995).
 37. This work is partially supported by NSF grant PHY-9018251 and NASA grants NAGW-1510 and NAGW-2376. Computations were carried out on the Cray C90 at the Pittsburgh Supercomputing Center and the CM5 system at the National Center for Supercomputing Applications. I thank S. Balbus, J. Stone, and S. Phinney for useful discussions and comments on the manuscript.

Turbulent Dynamics in the Solar Convection Zone

Nicholas Brummell, Fausto Cattaneo, Juri Toomre

Observations of the sun reveal highly complex flows and magnetic structures that must result from turbulent convection in the solar envelope. A remarkable degree of large-scale coherence emerges from the small-scale turbulent dynamics, as seen in the cycles of magnetic activity and in the differential rotation profile of this star. High-performance computing now permits numerical simulations of compressible turbulence and magnetohydrodynamics with sufficient resolution to show that compact structures of vorticity and magnetic fields can coexist with larger scales. Such structured turbulence is yielding transport properties for heat and angular momentum at considerable variance with earlier models. These simulations are elucidating the coupling of turbulent fluid motions with rotation and magnetic fields, which must control the interlinked differential rotation and magnetic dynamo action.

The outer layers of the sun are observed to be in continuous agitated motion because of vigorous turbulent convection. Theoretical models of stellar structure and evolution indicate that in the present sun some manner of thermal convection must extend from the surface well into the interior, forming a zone occupying about the outer 30% by radius in which convective motions transport nearly all of the energy that emerges from the radiative interior. Obser-

N. Brummell and J. Toomre are at the Joint Institute for Laboratory Astrophysics and the Department of Astrophysical, Planetary and Atmospheric Sciences, University of Colorado, Boulder, CO 80309-0440, USA. F. Cattaneo is at the Department of Astronomy and Astrophysics, University of Chicago, 5640 South Ellis Avenue, Chicago, IL 60637, USA.

ations suggest that the actual dynamics within this zone are extremely intricate. The velocities and magnetic fields are complex, exhibiting large-scale structure (Fig. 1A) and ordered behavior amidst rapidly varying and intense small-scale turbulence. High-resolution observations of the solar surface show that convection involves multiple and somewhat discrete scales of roughly cellular motion. The flows range from the fast and short-lived solar granules (Fig. 1C) with typical horizontal scales of 1000 km, through mesogranules with scales of about 5000 km, to fairly persistent supergranules (Fig. 1B) about 30,000 to 50,000 km across (1). It is so far unclear from theory as to how these different scales arise. Each of the convective flows tends to sweep and con-

centrate magnetic fields to the cell peripheries, forming loose networks of what appear to be compact magnetic flux tubes.

On the largest scale of motion, tracking of surface features shows that the sun does not rotate as a solid body. The differential rotation has a period of about 25 days at the equator, compared with about 33 days in the polar regions. The rotation rate of sunspots at mid-latitudes is somewhat faster than that of the surface plasma, suggesting that they may be rooted to more rapidly rotating fluid deeper down. Novel forms of observational data are beginning to provide guidance about some of the dynamics deeper in the convection zone. The recent field of helioseismology studies the nearly 10 million acoustic p modes of the interior that leak into the atmosphere where they can be observed (2). Inversion of their frequencies has permitted deductions to be made about the radial stratification throughout much of the sun, confirming that the sun is indeed nearly adiabatically stratified by the convection to a depth of about 200,000 km. Frequency splittings are in turn providing preliminary estimates of the variation of angular velocity Ω with both radius and latitude in the interior of the star. A surprising result is that the rotation profiles most commonly obtained from helioseismology (Fig. 2A) are at striking variance with expectations (Fig. 2B) based on earlier global simulations of solar convection.

The magnetic fields that emerge into the solar atmosphere are also remarkable in their diversity, and this must reflect how they are produced and shuffled by all scales of motion in the convection zone (3). The cyclic eruption of strong magnetic fields through the solar surface in the form of sunspots and active regions has long been a center of attention. The associated large-scale magnetic fields span a good fraction of the disk. Their signature in the solar corona is striking, for they appear as huge arcades or prominences of enhanced emission, as seen in the soft x-ray images from the Yohkoh satellite (Fig. 1A). At the surface in the quiet sun, virtually all the magnetic energy resides in compact flux elements or tubes, and these occupy only a small fraction of the surface area. The smallest of the detected compact magnetic structures are the bright points visible in the intergranular lanes in Fig. 1C.

The diversity of spatial and temporal scales present in the fluid motions and in the magnetic fields bespeak of a large-scale order achieved by what is seemingly a highly turbulent process. Major questions arise: In what manner do compressibility and stratification mold the character of turbulent convection? How does such turbulence interact with rotation and magnetic fields to produce the differential rotation of the

star and create dynamo action yielding cyclic magnetic activity? One route for coping with this is to avoid the fine details and appeal to statistical theories of turbulence from the outset (4). Another is to seek guidance from laboratory convection experiments (5). A third route, with possibly the greatest diagnostic potential, is to use numerical simulations. Attempting to answer such basic questions related to the sun has led to major efforts in computational fluid dynamics.

Role of Simulations

The explanation of how the large and small scales can coexist may be emerging from simulations that are capable of describing fully developed turbulent flows. Recent computational evidence (6) in various applications of turbulence theory indicates a surprising degree of structure (involving plumes and vortices, large-scale mean fields and flows, and zonal jets) embedded in otherwise chaotic flow fields, with significant consequences for the transport of momentum and energy and for the amount of dissipation. It appears that these coherent structures arise from self-organizing processes (inverse cascades) that can operate in highly turbulent systems. However, understanding the detailed dynamics of stellar convection raises fundamental difficulties for turbulence theory. The active scales of turbulence in the solar convection zone probably range from about 10^5 km (of order the depth of that zone) to 10^{-1} km or much smaller (estimates of viscous dissipation scales), encompassing at least six orders of magnitude for each physical dimension. The largest calculations bearing on solar convection are beginning to

deal with order 512^3 or 1024^3 spatial modes, capturing only about three orders of magnitude in each dimension. Such numerical modeling is just now becoming possible through the use of advanced computing resources provided within the national High Performance Computing and Communications (HPCC) initiative. That initiative has enabled interdisciplinary "grand challenge" teams of fluid dynamicists and computer scientists to work jointly on turbulence problems in geophysical and astrophysical fluid dynamics, using large vector and scalably parallel architectures to increase substantially the spatial resolution in three-dimensional (3D) simulations.

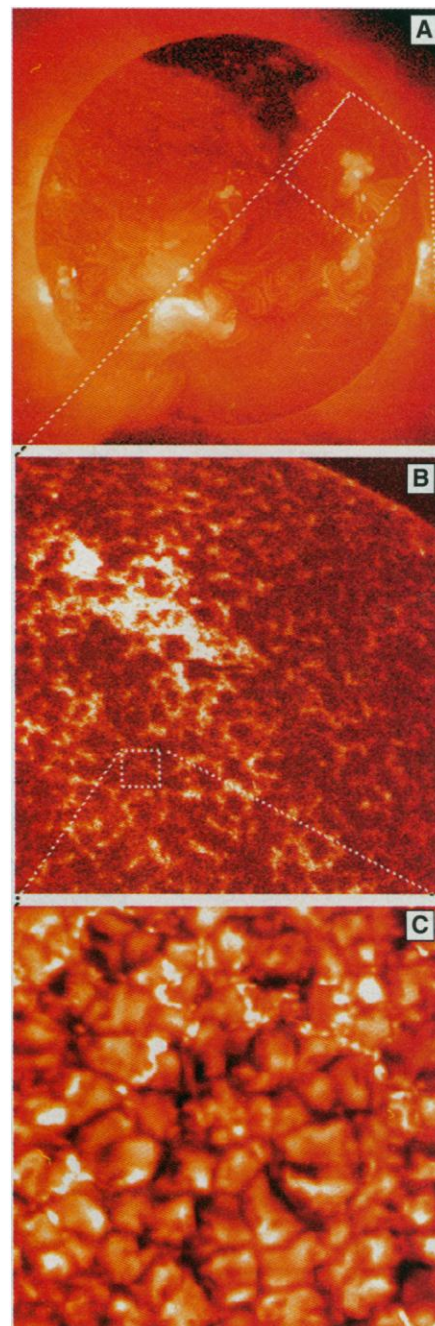


Fig. 1. (A) Image of the solar atmosphere from the Soft X-Ray Telescope (SXT) on the Yohkoh satellite, revealing enhanced emission from large magnetic field structures extending from the surface high into the corona (45). A coronal hole near the pole appears dark and is speckled by emission from small magnetic structures. (B) The strong horizontal flows of supergranulation sweep magnetic fields to their boundaries, yielding networks of enhanced emission in the ultraviolet C IV line, here observed with the Transition Region Camera (TRC) from a sounding rocket flight (46). The active region surrounding a sunspot also appears bright here. (C) High-resolution CH-bandhead intensity image observed under exceptional seeing conditions from La Palma, with effects of 5-min oscillations largely removed by digital processing, showing the intricate cellular patterns of solar granulation (47). In this region of relatively quiet sun, magnetic fields appear in the darker intergranular lanes as bright elements involving small but intense flux bundles, with the smallest about 100 km across. Boxes suggest relative sizes of each image, but the data are unrelated. [Images provided by the Lockheed Solar and Astrophysics Laboratory]

The most basic limitation at present is that the simulations cannot cope with the dynamical scales needed to resolve both granulation and global-scale circulations simultaneously. Further, the small viscosity and high electrical conductivity of the solar plasma, together with the large physical scales and flow speeds, imply that the kinetic and magnetic Reynolds numbers (7) are vast ($\geq 10^{12}$). The current 3D numerical simulations can reach at most moderate Reynolds numbers, which fall short of the solar values by six or so orders of magnitude. Therefore the numerical studies are not detailed solar simulations, but rather models to help develop our physical intuition about such complex dynamics. Several approaches have thus emerged in the design of numerical experiments related to solar convection, involving various compromises in their range of dynamical scales, the parameter regime, the geometry employed, or the detailed physics studied. We shall here turn to examples from recent simulations that are modifying our views about convection influenced variously by stratification, rotation, and magnetic fields, and discuss ideas about the magnetic dynamo action thus realized. We begin with global simulations that capture the full spherical geometry of

the convection zone in studying how differential rotation is established. We then turn to local models of compressible convection dealing with portions of that zone in order to achieve the higher spatial resolution necessary to study more turbulent states. Finally, we consider modeling approaches used to study the dynamics of solar magnetic fields.

Global Convection

Trying to understand the coupling of rotation with the larger scales of convection, and thereby address issues of differential rotation, meridional circulations, and eventually global dynamo action, requires study of a full spherical shell (8). The early numerical studies of such convection in rotating shells (9) were able to incorporate spherical harmonic expansions only up to degree $l \sim 30$. The convection that could be resolved was nearly laminar, and it was dominated by columnar roll-like cells (or "banana cells") oriented in the north-south direction (Fig. 2C). The tilting of these cells produces Reynolds stresses that drive zonal flows, which appear as differential rotation (Fig. 2B). The simulations (10) yield a nearly constant angular velocity Ω along the axes of the columnar cells and

thus a nearly constant Ω on cylinders aligned with the rotation axis, decreasing with depth in the equatorial plane. The sun does not appear to comply. As commonly judged so far from helioseismic observations (Fig. 2A), its angular velocity at high latitudes increases with depth, at mid-latitudes is nearly constant on radial lines, and near the equator first increases and then gently decreases with depth (2, 11). Thus, there appears to be a major discrepancy in Ω between early convection theory and helioseismic deduction. Similar columnar convection has also been seen in the Geophysical Fluid Flow Cell (GFFC) electroconvection experiment flown on Spacelab 3, which studied rotating spherical shells of fluid in the presence of a simulated radial gravity field (12), although far more complicated turbulent flows were also established with stronger driving. The disparity in the simulations may result from the models being capable of describing only laminar flows.

Recent spherical shell simulations performed with HPCC resources have attained a spatial resolution about 10-fold greater in each dimension (13), extending to $l \sim 320$ while typically restricting the domain to a 45° wedge in longitude (with periodic boundary conditions on meridian planes). With the increased nonlinearity that is thereby possible, the resulting convection is highly time dependent and the flows are quite intricate: The snapshot in Fig. 3 shows much less evidence in temperature or radial velocity fields of the earlier banana cells. The convection is now dominated by intermittent plumes of upflow and downflow, with the downflows stronger in amplitude, although there is still some semblance of north-south alignment of structures in the equatorial region. The temperature fluctuations possess some zonal banding near the top of the layer; warmer zones are

Fig. 2. (A) Contours of angular velocity Ω in a meridional plane in the solar interior, deduced from helioseismic data (2, 11). The axis of rotation is vertical. Bottom of convection zone is shown dashed; labels of $\Omega/2\pi$ are in microhertz. (B) Contours in a meridional plane of angular velocity from an early anelastic spherical shell convection simulation. The equatorial region rotates faster than the poles, but Ω is constant on cylinders. (C) A snapshot of the radial velocity patterns in the form of "banana cells" is shown on a spherical surface in the upper part of the simulation (10).

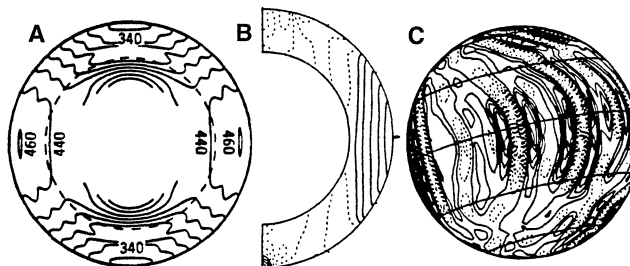
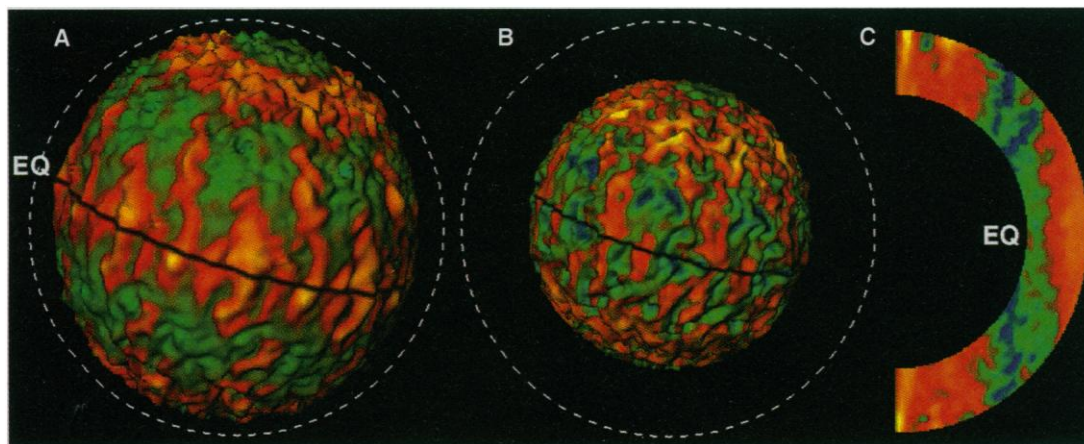


Fig. 3. Spherical shell modeling of anelastic turbulent rotating convection (48), showing a snapshot of the radial velocity and temperature fluctuations on a spherical surface (A) near the top of the layer and (B) near the bottom. Radial velocity defines the distortions of the surface, and temperature fluctuations color it; red-yellow tones are warmer and green-blue tones cooler than the mean. Dashed circle outlines full domain. With increased nonlinearity, columnar cells have largely broken up and have been replaced by more irregular convection. (C) Contours of the mean zonal velocity (relative to the rotating frame) shown in a meridional plane, with red-yellow tones being prograde, blue-green retrograde. Prograde motion (fast) exists at low latitudes, with a belt of retrograde



motion (slow) at mid-latitudes and a polar vortex of prograde motion (fast) near the poles. Such differential rotation is only roughly symmetrical about the equator. [Simulation by Glatzmaier and Toomre, imaging by Goldstein]

near the equator and at higher latitudes with only the latter surviving near the bottom of the layer (14). Some zonal thermal banding has also been observed through solar irradiance measurements (15) and appears to have been detected at greater depths with helioseismic time-distance analyses of acoustic wave fields (16). The latitudinal positioning of the warmer bands is somewhat different in the models and the observations, with the latter possibly favoring the evolving latitudes at which sunspots emerge during the 11-year cycles. The accompanying mean zonal flow profiles (Fig. 3C) of the simulations, while still showing a columnar tendency, now exhibit finer scale shearing features. The angular velocity at mid-latitudes hardly varies with depth (so is almost constant on radial lines), but at low latitudes it decreases gradually with depth. Although the puzzles of differential rotation and thermal banding have hardly been resolved, such global simulations appear to offer a promising theoretical path to be pursued further with even better spatial resolution.

Rotating Local Models

A major trade-off exists between assigning the computationally available degrees of freedom to modeling the full spherical geometry or to resolving the range of scales associated with the turbulence. Even with current technology, the global models of convection can operate only in the mildly turbulent regime, and thus predictions about the differential rotation profiles that can result in the sun are still rather uncertain. In contrast, local models restrict the domain to small (but still three-dimensional) subsections of the global domain, channeling all of the available resources into the numerical resolution of the most turbulent parameter regime possible. The effort is then to understand the differences between

the transport properties of turbulent and laminar flows.

There have been substantial thrusts in local modeling of fully compressible convection in 3D, rectilinear Cartesian slab geometries (17). Recent work has incorporated f -plane rotation (18), wherein an angular velocity vector that is constant throughout the domain generates Coriolis forces on the fluid. The rotation vector and gravity are not necessarily aligned, representing a planar layer positioned tangentially to the rotating sphere at some latitude ϕ . Such simulations of rotating convection have primary bearing on supergranular and larger scales of motion on the sun, for their circulation time scales become long enough compared to the solar rotation period that such flows are influenced by Coriolis effects.

Increasing the degree of turbulence (7) in such simulations reveals a dramatic transition away from laminar, slowly overturning flow throughout the domain. The upper surface remains a connected network of downflows surrounding broad upflows, similar in appearance to solar surface granular flows, but it disguises highly turbulent flows below (Fig. 4A). The turbulent interior consists of fast, small-scale, isotropic motions. The seemingly smooth cellular flow in the surface region is a consequence of the expansion of fluid elements rising through a rapidly decreasing density stratification near the upper boundary. Powerful downflows occur at the interstices of the upper network and pierce the interior turbulence, spanning the multiple density scale heights of the domain. Despite their mobility, these strong downflowing structures are spatially and temporally coherent, coexisting with the interior turbulence for many turnover times.

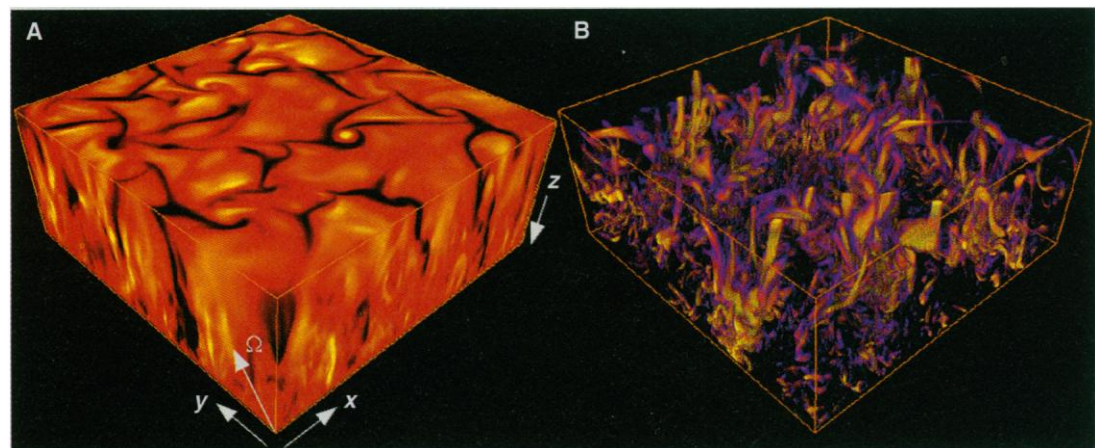
The turbulent yet structured nature of the flow is characterized most clearly in terms of the vorticity (the localized spin of fluid elements) (19) (Fig. 4B). The coher-

ent downflows are strong, sizable vortex chimneys (Fig. 5A) that punctuate the interior, where they are buffeted by much smaller, randomly orientated vortex tubes (Fig. 5B). Rotation intensifies these signatures, providing a source of intrinsic vorticity for the coherent structures and a linear mechanism (20) for mixing the small-scale vorticity components. Such turbulent interior dynamics could not be anticipated nor understood from the majority of solar observations, which sense only flow properties near the surface. The simulations suggest that persistent large-scale structures may well exist amidst intense small-scale turbulence at greater depths within the solar convection zone, and these might be searched for with helioseismic techniques.

These local models of turbulent rotating convection, involving coherent structures interacting with small-scale disordered motions, also possess distinctive transport properties for both angular momentum and heat. In such a local model, the horizontally averaged mean velocities $\bar{u}(z)$ and $\bar{v}(z)$ (z is depth) are analogous to the zonal and meridional mean flows of the full spherical shell. These shear flows are generated from Reynolds stresses by correlations of vertical and horizontal motions. With the rotation vector tilted away from gravity in a longitudinal plane, as for the f -plane model positioned away from the pole, the rotation has both a vertical and a meridional component. With smooth, laminar overturning motions, the meridional component acts preferentially on the zonal motions, tilting the cells to provide a correlation between the zonal flows and the vertical velocities, and thus serves as a source term for strong shearing mean zonal flows (21).

The turbulent case here is very different. The small-scale isotropic motions tend to feel the rotation only weakly because they turn over too fast in comparison to the rotation time, leaving only the

Fig. 4. (A) Perspective view of a typical solution from a 3D local model of turbulent compressible convection with rotation (49). The tilted rotation vector Ω is indicated. Vertical velocities are shown near the boundaries of the domain, with lighter tones indicating upward motions and darker tones downward flows. Note the cellular network near the upper surface, with structures penetrating the whole depth visible on the sides, and smaller scale motions in the interior. (B) Volume rendering of enstrophy (vorticity squared) of the same full domain, with a color and an opacity assigned to each enstrophy value. Bright and opaque colors represent strong enstrophy; dark and translucent are weak. Apparent are the strong chimneys associated with



the coherent structures and the vortex tubing in the interior. [Simulation by

Brummell, Hurlburt, and Toomre]

coherent structures with significant vertical and temporal coherence to experience the rotational effects. These vortex structures tend to align with the rotation vector in a balance akin to the Taylor-Proudman constraint (22) (Fig. 6A). This turbulent alignment then preferentially correlates vertical and meridional motions, contrary to the laminar case. The weakened mean zonal flows become independent of depth, yielding a nearly constant but significant \bar{u} throughout the interior, closer to the spirit of the helioseismic deductions (Fig. 2A) than the earlier global solar models. The balance between the cellular and turbulent alignments in the local models provides constant mean zonal flows in the interior that vary in magnitude with latitude (Fig. 6B) and even spiral with depth (Fig. 6C), somewhat in accord with the recent helioseismic inferences (23) from analyses of acoustic wave fields over localized areas on the sun. Soon, helioseismic methods based on such

ring diagram and phase analyses (24) may provide the means to detect mean flows and possible coherent structures deep within the convection zone.

The transition to turbulence in the local models also has consequences for the heat transport. Even though the strong downflowing structures communicate over many scale heights and are coherent in time and space, remarkably the small-scale turbulent motions carry the majority of the vertical convective flux. The coherent structures are so organized that their strong kinetic flux directed downward very nearly counterbalances their enthalpy or heat flux upward (in a horizontal average), rendering them relatively inefficient. The major transport is left to the smaller turbulent motions of the interior. Thus, if the convection is sufficiently turbulent, these local models suggest a surprising new picture in which the large-scale coherent motions serve primarily to organize the convective circulations and

the majority of the net convective transport is achieved by the small-scale turbulent motions. This result may bear on the apparent successes of simple mixing-length approaches (25).

Other local models are used in attempts to understand convection near the surface of the sun, seeking to provide dynamical descriptions for what occurs on the scales of granulation and mesogranulation. The surface represents a transition from a highly unstable interior to a very stable atmosphere above, and thus serves as a complicated penetrable boundary layer with rapidly varying fluid and radiative properties. The physics needed to describe flows near the surface—where radiative transfer and realistic equations of state, opacities, and ionization changes should be dealt with in detail—is much more complex than the physics of nearly perfect gases. The local modeling of granulation makes use of a computational domain in the vertical that encompasses both the upper portion of the

Fig. 5. Volume rendering of the enstrophy in Fig. 4B in shallow horizontal segments viewed from above for (A) the upper eighth of the domain and (B) the bottom eighth, with the positive (warm only) temperature fluctuations overlaid in red-yellow tones. Near the top, double vortex sheets are present in the downflow networks surrounding the broad, warm upflowing regions, with strong vertical vortices often positioned at the interstices of the network. Intense small-scale vortex tubes characterize the interior, embedded in broader temperature structures. [Simulation by Brummell, Hurlburt, and Toomre]

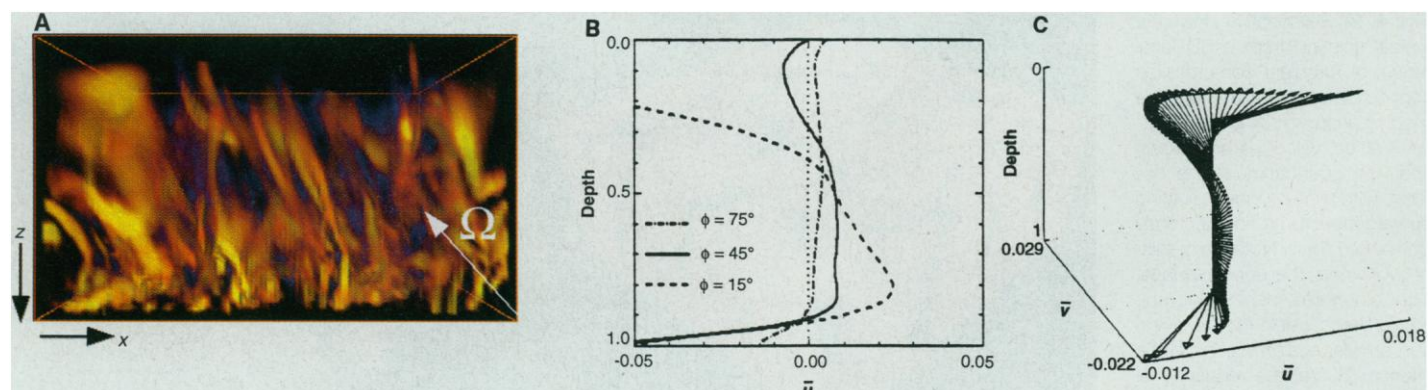
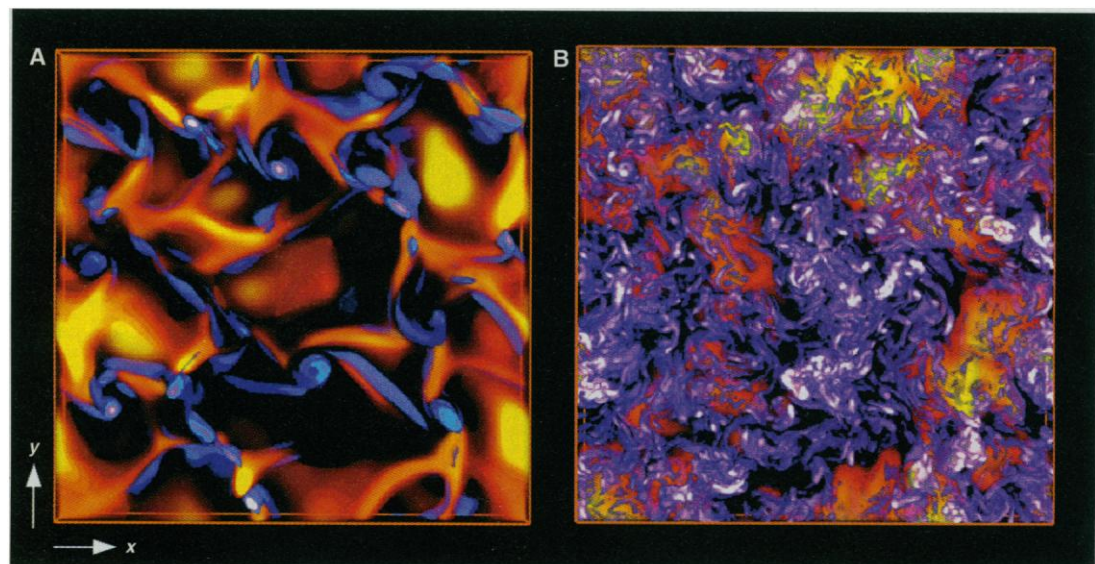


Fig. 6. (A) Enstrophy volume rendered from the side of the layer for a turbulent case with strong rotation (50), showing the alignment of coherent structures with the rotation vector Ω over much of the depth of the layer. (B) Mean zonal flows produced with the local f -plane model at various latitudes ϕ , exhibiting the

weak but constant mean flow generated in the turbulent interior. Velocities \bar{u} and \bar{v} are scaled by the sound speed; proportional depth is shown. (C) Spiraling of the total mean flow vector with depth (with inertial oscillations removed). [Simulation by Brummell, Hurlburt, and Toomre]

solar convection zone and the lower atmosphere (26). Such modeling is still restricted to mildly turbulent flows, unlike those in the sun itself, yet the resulting vigorous convection at the surface (Fig. 7A) is overall strikingly similar to that in perfect gas models and to the best observational images of granulation (Fig. 7B). However, the latter suggest the presence of a broader range of small scales, consistent with much higher Reynolds numbers, which characterize the real solar turbulence.

Intensely Turbulent Convection

The properties of convective turbulence are sensitive to the rates at which vorticity is diffused by viscosity and at which temperature is diffused by thermal conductivity. That ratio of coefficients is the Prandtl

number Pr . With $Pr \lesssim 0.1$, vortex stretching is important and results in substantial complexity of the flows. The gaseous medium of the solar convection zone has $Pr \sim 10^{-8}$, and so in the quest to study convective turbulence at low effective Pr , local models have also used the piecewise-parabolic method (PPM) to solve the Euler equations of inviscid, compressible fluid flow (27). The viscosity of the perfect gas is provided solely by the numerical viscosity in the PPM code, and on fine spatial grids, that viscosity is small, yielding Pr of order 10^{-4} at this stage.

Local modeling of convection with the PPM algorithm (so far ignoring rotation) yields flows that are highly turbulent yet exhibit a large-scale order that evolves in time (28). The rendering of enstrophy (vorticity squared) near the top boundary (Fig.

8A) reveals quite striking vorticity structuring. Long horizontally orientated pairs of counterrotating vortex tubes are produced with the initiation of a downflow lane, and their instabilities lead to various intricate structures, including vortex rings. There is substantial lateral advection of such vortex structures into a larger scale downflow network. Slightly deeper (Fig. 8B), the main downflow system becomes evident as a large circulation pattern is formed and laced with small-scale vorticity structures. The downflowing coherent structures are now highly turbulent, amidst regions of turbulent upflow (29).

The flows in the PPM simulations possess considerably higher Reynolds numbers Re than the other solutions shown and are correspondingly far more complicated. In these models, the larger downflow systems are themselves turbulent, being interspersed with small-scale vortex tubes. This suggests that the prominent downflow lanes seen in granulation images (Fig. 1C) might well be regions of intensely chaotic small-scale flow. It is unfortunate that the vorticity of granules is unobservable. Further, all the compressible simulations have shown that there is a natural large-scale pattern that arises from the coherent downflow networks. Such patterns extend over many density scale heights and therefore become more evident with depth. Their presence indicates that convective turbulence tends to self organize and build large structures among small-scale random motions. Such processes provide hints for how the multiple scales of granulation, mesogranulation, and supergranulation in the sun might come about, although the discrete depths at which hydrogen and helium are ionized may also lead to preferential driving of such different scales of convection in the sun.

Fig. 7. (A) Simulation of solar granulation (26), showing the plan view in the horizontal of emergent intensity in the surface layers at one instant in time. The field of view is broadened by adjoining another intensity image slightly shifted in time. The basic rectilinear computational domain is 6000 km wide in the horizontal and 3000 km in the vertical, resolved with 253^2 by 163 spatial modes. (B) For comparison, shown to same scale is an intensity image observed in the CH-bandhead from La Palma (47). If the simulation image were adjusted to account for atmospheric seeing distortions, these two images would be qualitatively similar. [Simulation by Nordlund and Stein]

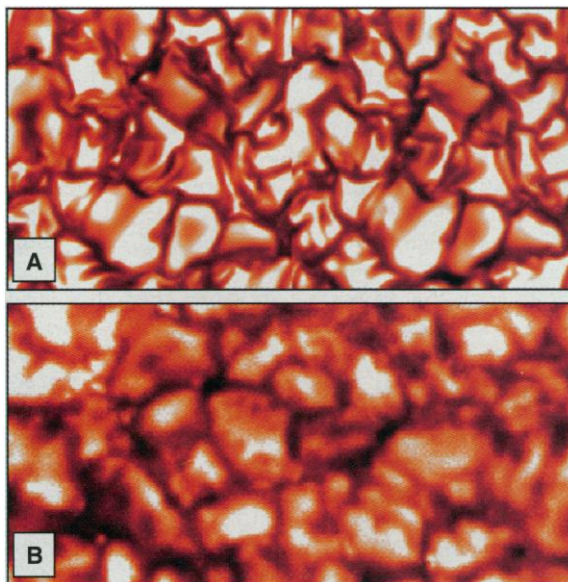
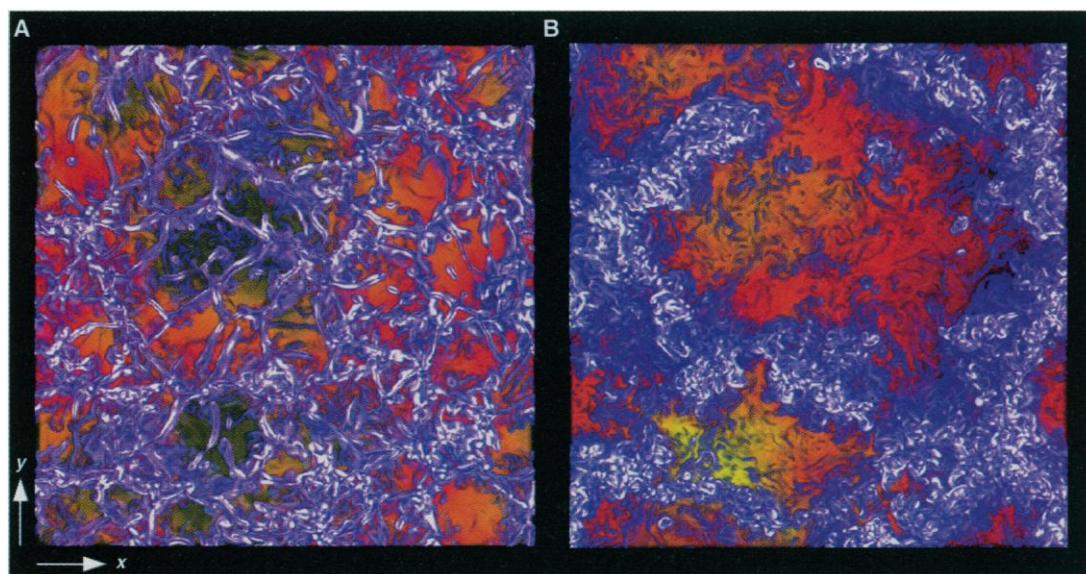


Fig. 8. Enstrophy volume rendered at one instant in time in the PPM intensely turbulent convection simulation (51). Enstrophy is shown in two shallow horizontal segments viewed from above, augmented by positive temperature fluctuations in red-yellow tones: (A) near the top boundary, and (B) second pressure scale height from the top. Strong vortex tubes (primarily associated with downflow lanes) are apparent near the upper surface, and these exhibit intricate and rapidly varying secondary instabilities. The strong downflow network laced with small-scale vortex tubes becomes evident in the interior of the layer. [Simulation by Porter and Woodward, imaging by Brummell]



The high effective Re of the PPM simulations yields large dynamic fluctuations in space and time. The transport properties are therefore highly variable, and the pointwise thermodynamic fluxes are often 100-fold greater than the mean. Despite such strong intermittency, the fluxes in the downflowing structures still exhibit a remarkable degree of cancellation in horizontal means, leaving the upflows to carry typically about two-thirds of the total convective flux (30). Although the tendency for the kinetic and enthalpy fluxes to cancel in the downflows is not so pronounced, here too the net convective transport achieved by the prominent large-scale coherent structures is modest compared with that by the smaller scales.

Solar Magnetic Fields and Dynamo Action

The solar magnetic field also presents a striking but now familiar dichotomy. At small scales it appears to be random. High-resolution magnetograms of the solar surface show a high degree of spatial intermittency, such that most of the field is concentrated in narrow flux elements surrounded by almost field-free plasma (3). In the quiet sun, these elements are present in greater or smaller number all over the solar surface; both field polarities occur roughly with equal likelihood, giving magnetograms a familiar "salt and pepper" look. The time variability of this small-scale component is also random. The pattern formed by the regions of moderate magnetic field intensity (≤ 1000 G, say) evolves on time scales of a few minutes, comparable to the coherence time of the granular flows. In regions of extreme concentration like pores or sunspots, the magnetic field can become strong enough (several thousand gauss) to alter the ambient flow substantially (31). These stronger magnetic structures can maintain their identity for up to several weeks.

On larger scales and longer times, the picture changes dramatically. The 11-year solar activity cycle becomes evident in the release and morphology of magnetic flux. At the beginning of the cycle, new magnetic flux in the form of active regions emerges at mid-latitudes. The typical active region consists of two well-formed sunspots surrounded by small-scale magnetic elements. The two spots are roughly oriented east-west and have a small inclination angle that changes systematically during the course of the cycle. The order of the polarity of the sunspots (for example, plus for the leader spot, minus for the follower spot) is opposite in the two hemispheres and is preserved during the cycle. As the cycle progresses, the emergence rate first increases, then decreases, and the emergence latitude slowly

drifts toward the solar equator. Eventually a new cycle begins, with flux emerging again at mid-latitudes but with the polarity law reversed (32).

The statistical stability of the period of the solar cycle, the existence of a well-defined polarity law, and the systematic variation of the angle of tilt for sunspot pairs all indicate that the solar magnetic field is not simply a random process. Even though on small scales it appears disordered, on large scales it presents a remarkable degree of organization. Further, the reversal of the large-scale component of the field indicates that all the magnetic flux must be processed in an 11-year period. Namely, the solar field cannot be primordial but must be destroyed and regenerated every cycle. How magnetic fields are generated by the turbulent motions in the convection zone and become organized into large-scale coherent structures that manifest themselves as the activity cycle is the central problem of solar dynamo theory.

The spatial character of the solar cycle suggests the existence of a large-scale toroidal field located in the lower part of the convection zone, or possibly at the interface between the convection zone proper and the radiative interior, that is of opposite polarity in the two hemispheres. Magnetic flux rises through the convection zone and emerges as active regions as a result of instabilities of this large-scale structure; the east-west orientation of sunspot pairs is a signature of the orientation of the underlying magnetic field. Some of these ideas have recently been made more quantitative by a series of numerical simulations based on the thin flux tube approximation (33). Initially, the field is assumed to be in the form of slender toroidal loops that evolve subject to the Coriolis force, buoyancy, magnetic tension, drag, and the constraint of transverse pressure balance. In this framework, the flux tubes become geometrical objects with no internal structure and are essentially decoupled from the ambient turbulence. This approach has successfully

reproduced many features of the solar cycle and, furthermore, has predicted that in order for magnetic flux to emerge at the observed latitudes with the (bipolar) active regions having the correct tilt with respect to the equator, the underlying toroidal field must be of order 10^5 G (Fig. 9) (34). This value exceeds the estimated equipartition strength, the value at which the kinetic and magnetic energy densities are the same, by roughly one order of magnitude. The generation of such strong coherent fields is theoretically not straightforward.

A toroidal field can be generated from a poloidal one by the winding action of differential rotation (31), although it is sensitive to details of the rotation profiles. The inverse process, involving the generation of a poloidal field from a toroidal one, is much more subtle. One of the great successes of mean-field electrodynamics has been to provide the theoretical foundation for precisely such a mechanism, the α effect (35). The basis for this effect is that a localized helical deformation of a mean field gives rise to an isolated current contribution, and under suitable circumstances, many of these contributions may add to produce a net mean current parallel to the mean field. The resulting inductive effect can then act as a source term for the poloidal field. In order for the average effect to be nonzero, the underlying field of turbulence must have a definite handedness, as is the case for flows in rotating objects. Also, the α effect requires some irreversible process like diffusion (36). The classical (ohmic) decay time for the solar dipole component, say, is comparable to the age of the sun itself. However, because all of the magnetic flux must be processed in roughly 11 years, some form of enhanced diffusion must be operating. For this enhancement to be possible, gradients of magnetic field and hence magnetic fluctuations must be substantial (37).

Considerable progress has been made recently in the study of the geometrical properties of magnetic fluctuations in the context of

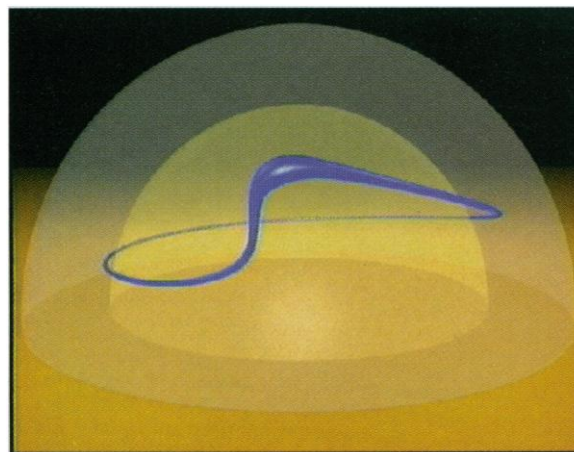


Fig. 9. Simulation of an emerging magnetic loop of equipartition strength based on the slender flux tube approximation (34); the axis of rotation is vertical. The translucent hemispheres correspond to the inner and outer boundaries of the convection zone. In this particular case, the magnetically induced buoyancy of the loop is not sufficient to overcome the effects of the Coriolis force, and thus, the loop emerges at a high latitude. [Simulation by Caligari, Moreno-Insertis, and Schüssler]

the fast-dynamo problem (38). A fast dynamo, by definition, is one whose (positive) growth rate becomes independent of diffusion in the limit of zero diffusion. Thus, a fast dynamo operates on the dynamic rather than diffusive time scale. The study of this kind of dynamo is motivated by the astrophysical limit where the diffusive time scale greatly exceeds the dynamical time scale (nine orders of magnitude in the sun and as many as 12 in a typical galaxy) (39). A prediction of this theory, confirmed by numerical experiments, is that as the diffusivity decreases, the magnetic fields develop increasingly finer structure and fluctuate both in amplitude and sign on finer and finer scales (Fig. 10) (40). Another property of fast-dynamo fields is that for wide classes of velocities, the strength of the fluctuations greatly exceeds that of the mean (41). This presents an interesting problem. On the one hand, flux-tube simulations indicate that the mean field must exceed equipartition in order for the spatial pattern of the activity cycle to agree with observations. On the other hand, fast-dynamo calculations show that for diffusion to operate, the fluctuations must be considerably stronger than the mean, leading to the conclusion that the magnetic fluctuations must greatly exceed equipartition, possibly by many orders of magnitude. This latter conclusion is at odds with our intuitive notions of what is energetically possible (37, 42). Thus, one of the problems of present solar dynamo theory is how to reconcile the existence of a strong, coherent mean field with the requirement of irreversibility and strong fluctuations.

Two possible resolutions have been proposed. One is that the magnetic field is in fibril form, involving thin flux tubes. Irreversibility occurs through reconnection

events between flux tubes, and therefore, the energetic considerations based on diffuse fields do not apply. The other is that as the magnetic field grows in amplitude, the Lorentz force modifies the underlying field of turbulence and the resulting nonlinear state is not related to the kinematic eigenfunctions of fast dynamo theory (43). With our present knowledge, it is difficult to give preference to either theory. Which, if any, is more realistic will perhaps be settled by the next generation of numerical simulations. However, it will still be some time before the dynamo action of these simulations can be linked with the full dynamics, including feedback to the differential rotation, such that a cogent theoretical description of the full dynamo system emerges.

Conclusions

Though still far from the full dynamical range of the solar convection zone, the recent numerical simulations with their extended diagnostic ability are providing an understanding of the underlying physical mechanisms. Such ventures are showing how large-scale coherent structures and strong mean flows can coexist with intense small-scale turbulence. The presence of the more ordered convective flow structures that can span many density scale heights in the vertical, combined with seemingly incoherent smaller scales involving intense vortex tubes, has a substantial influence on the transport of both heat and angular momentum. Recent modeling of dynamo processes similarly suggest that larger scale coherent magnetic structures can coexist with intermittent small-scale fields. The scalability of these 3D simulations to ever faster

vector and scalably parallel machines with larger memories holds out hope for major advances in dealing with the intricate dynamics of multiple turbulent scales.

Such numerical simulations concentrate on the sun because its nearness provides detailed observations that can both inspire and seriously test the theoretical efforts. The continuing advances in high-resolution observations of the solar surface serve to emphasize the diversity of scales present in both the velocity and magnetic fields, and they will provide a major challenge to the turbulence simulations. Other input comes from helioseismology, which provides indirect measurements of large-scale flows, including differential rotation, throughout the convection zone. If one uses the giant planets Jupiter and Saturn as a guide, which also are vigorously convecting as they rotate, then one might well expect that the sun also possesses strong zonal jets and structured flows in its convection zone, in addition to broader variations of differential rotation. Far more detailed deductions about subsurface solar flows (2, 44) can be expected in the next few years as nearly continuous helioseismic observations become available both from the ground-based, six-station Global Oscillations Network Group (GONG) project, which starts full operations in October 1995, and from the space-based, Doppler-imaging high-resolution instrument Solar Oscillations Investigation-Michelson Doppler Imager (SOI-MDI) on the Solar Heliospheric Observatory (SOHO) spacecraft to be launched shortly thereafter. Similarly, the scheduled reflight of the GFFC experiment on the shuttle mission USML-2 in September 1995 promises to provide images of turbulent structures realized with rotating spherical convection. Thus, there is likely to be ample input in the near future from major observational and experimental studies that can serve to guide and challenge these computational ventures in astrophysical fluid dynamics.

REFERENCES AND NOTES

1. H. C. Spruit, Å. Nordlund, A. M. Title, *Annu. Rev. Astron. Astrophys.* **28**, 263 (1990).
2. D. O. Gough and J. Toomre, *ibid.* **29**, 627 (1991).
3. P. A. Gilman, in *Physics of the Sun*, P. A. Sturrock, T. E. Holzer, D. M. Mihalas, R. K. Ulrich, Eds. (Reidel, Dordrecht, Netherlands, 1986), vol. 1, pp. 95-160; S. K. Solanki, *Space Sci. Rev.* **63**, 1 (1993).
4. Modified mixing-length and anisotropic-diffusion models can be used to estimate Reynolds stresses of rotating convection that can serve to drive global-scale flows, for example, G. Rüdiger, *Geophys. Astrophys. Fluid Dyn.* **16**, 239 (1980); G. Belvedere, L. Paterno, M. Stix, *Astron. Astrophys.* **86**, 40 (1980); D. H. Hathaway, *Astrophys. J.* **276**, 316 (1984); B. R. Durney, *ibid.* **378**, 378 (1991).
5. Recent laboratory convection experiments deal with transitions from "soft" to "hard" turbulence that yield distinctive changes in heat transport, for example, B. Castaing *et al.*, *J. Fluid Mech.* **204**, 1 (1989); E. D. Siggia, *Annu. Rev. Fluid Mech.* **26**, 137 (1994). Other experiments study rotating shells of turbulent convection to ascertain the ordering and stability of flow patterns, for example, C. R. Carrigan and F. H. Busse, *J. Fluid Mech.* **126**, 287 (1983); J. E. Hart, G.

Fig. 10. Simulation of dynamo action at high magnetic Reynolds number ($\sim 10^5$) in the kinematic regime. The magnetic field intensity normal to the plane of the paper is shown on a cut through the computational domain. The solution was obtained by a Lagrangian method that tracks individual fluid trajectories (1024^2 in this case). Black and white regions correspond respectively to the peak values with opposite polarity. This illustrates the extreme spatial intermittency and the complex geometry of the magnetic fluctuations in the limit of small magnetic diffusivity. [Simulation by Cattaneo and Kim]



- A. Glatzmaier, J. Toomre, *ibid.* **173**, 519 (1986).
6. Z.-S. She, E. Jackson, S. A. Orszag, *Nature* **344**, 226 (1990); U. Frisch and S. A. Orszag, *Phys. Today* **40**, 24 (January 1990); J. C. McWilliams, *J. Fluid Mech.* **219**, 387 (1990); A. Vincent and M. Meneguzzi, *ibid.* **225**, 1 (1991); D. H. Porter, A. Pouquet, P. R. Woodward, *Phys. Rev. Lett.* **68**, 3156 (1992); *Phys. Fluids* **6**, 2133 (1994); K. Julien, S. Legg, J. McWilliams, J. Werne, in preparation.
 7. The Reynolds number Re is defined as UL/ν , where U is a typical velocity, L a length scale, and ν the effective fluid viscosity. A global Re may be estimated by taking U to be the root mean square (rms) of the velocity over the turbulent domain and L as the scale of the largest energetic flows. Using the Taylor microscale λ for L , which characterizes the scale of viscous dissipation at the rms velocity, yields Re_λ , and this is often used for intercomparison of the intensity of turbulence realized. Replacing the fluid viscosity by the electrical conductivity yields a magnetic Reynolds number.
 8. A favored technique is to expand the horizontal structure in terms of spherical harmonic functions Y_l^m (of degree l and order m), thereby obtaining uniform resolution on the sphere, and to simplify the physics by using a perfect gas. Anelastic filtering is used to avoid having to resolve sound waves while still retaining effects of density stratification. The shell of unstable fluid is confined by stress-free upper and lower boundaries, with a fixed temperature on the upper one and an imposed heat flux on the lower one. The strength of buoyancy driving and effects of rotation can be varied with the dimensionless parameters of Rayleigh number Ra , Prandtl number Pr , Taylor number Ta , and effects of stratification by the density contrast χ across the layer. The effects of rotation on the resulting convection can be measured by a convective Rossby number, $Ro = (Ra/TaPr)^{1/2}$; values of order unity or less suggest strong rotational constraints.
 9. G. A. Glatzmaier, *Astrophys. J.* **291**, 300 (1985); P. A. Gilman and J. Miller, *Astrophys. J. Suppl.* **61**, 585 (1986). Magnetic dynamo action has been assessed in such global modeling by G. A. Glatzmaier [*Geophys. Astrophys. Fluid Dyn.* **31**, 137 (1985)].
 10. G. A. Glatzmaier, in *The Internal Solar Angular Velocity*, B. R. Durney and S. Sofia, Eds. (Reidel, Dordrecht, Netherlands, 1987), pp. 263–274.
 11. K. G. Libbrecht, *Astrophys. J.* **336**, 1092 (1989); T. M. Brown *et al.*, *ibid.* **343**, 526 (1989); W. A. Dziembowski, P. R. Goode, K. G. Libbrecht, *ibid.* **337**, L53 (1989).
 12. J. E. Hart *et al.*, *Science* **234**, 61 (1986); J. Toomre, J. E. Hart, G. A. Glatzmaier, in (10), pp. 27–44.
 13. G. A. Glatzmaier and J. Toomre, *Astron. Soc. Pac. Conf. Ser.* **76**, 200 (1995); in preparation.
 14. A weak meridional circulation with outward flow in the equatorial region advects warm fluid outward to yield the warmer band there. This circulation is maintained by Coriolis forces that result from the zonal flows, which themselves are driven by Reynolds stresses of the turbulent convection.
 15. J. R. Kuhn and K. G. Libbrecht, *Astrophys. J.* **381**, L35 (1991); J. R. Kuhn, *Astron. Soc. Pac. Conf. Ser.* **42**, 27 (1993).
 16. T. L. Duvall Jr., S. M. Jeffries, J. W. Harvey, M. A. Pomerantz, *Nature* **362**, 430 (1993); T. L. Duvall Jr., *Astron. Soc. Pac. Conf. Ser.* **76**, 465 (1995); _____, S. M. Jeffries, J. W. Harvey, J. Schou, S. D'Silva, in preparation.
 17. These models place a perfect gas in a rectilinear domain considered periodic in the horizontal directions and bounded in the vertical by stress-free walls. A constant heat flux is applied from below and the upper surface is kept at constant temperature. Cartesian coordinates are used, with x and y in the horizontal directions and z increasing with depth. The codes solve the partial differential equations of fully compressible motions using pseudospectral techniques in the horizontal and finite differences in the vertical. Resolutions up to 256^3 have been used. See F. Cattaneo, N. H. Brummell, N. E. Hurlburt, A. Malagoli, J. Toomre, *Astrophys. J.* **370**, 282 (1990); A. Malagoli, F. Cattaneo, N. H. Brummell, *ibid.* **361**, L33 (1990). Related simulations are reported by K. L. Chan and S. Sofia, *ibid.* **336**, 1022 (1989); M. Hosain and D. J. Mullan, *ibid.* **380**, 631 (1991).
 18. N. H. Brummell, N. E. Hurlburt, J. Toomre, in preparation. See also *Astron. Soc. Pac. Conf. Ser.* **42**, 61 (1993); N. H. Brummell, X. Xie, J. Toomre, C. Baillie, *ibid.* **76**, 192 (1995). The f -plane model has also been used in the weakly nonlinear compressible regime by P. Pulkkinen, I. Tuominen, A. Brandenburg, Å. Nordlund, R. F. Stein [*Astron. Astrophys.* **267**, 265 (1993)] and for Boussinesq convection by D. H. Hathaway and R. C. J. Somers [*J. Fluid Mech.* **164**, 91 (1986)] and K. Julien, S. Legg, J. McWilliams, and J. Werne (in preparation).
 19. Vorticity is defined as the curl of the velocity vector field, and enstrophy is a scalar variable of the vorticity amplitude squared.
 20. The Coriolis term $\Omega \times \mathbf{u}$ in the momentum equations can redistribute energy between the components of the flow, whereas without rotation this can only be achieved by the nonlinear terms.
 21. Tilting of cellular flow leading to mean flows can result spontaneously from an instability [L. N. Howard and R. Krishnamurti, *J. Fluid Mech.* **170**, 38 (1986); N. H. Brummell and K. Julien, in preparation] but can be enhanced by the constraining effects of other processes such as rotation and magnetic fields [N. H. Brummell and J. E. Hart, *Geophys. Astrophys. Fluid Dyn.* **68**, 85 (1993); A. M. Rucklidge and P. C. Matthews, in *Solar and Planetary Dynamics*, M. R. E. Proctor, P. C. Matthews, A. M. Rucklidge, Eds. (Cambridge Univ. Press, Cambridge, 1993), pp. 257–264].
 22. J. P. Pedlosky, *Geophysical Fluid Dynamics* (Springer-Verlag, New York, 1979), p. 43. The Taylor-Proudman constraint in the limit of low Rossby number and vanishing viscosity suggests that flows should be invariant in the direction of the rotation axis. The conditions do not strictly apply here but a similar balance is achieved, except that motions spiral parallel to the rotation vector.
 23. J. Patron, F. Hill, E. J. Rhodes Jr., S. G. Korzennik, A. Cacciani, *Astron. Soc. Pac. Conf. Ser.* **76**, 208 (1995).
 24. Ring diagram methods applied to local wave fields are discussed by F. Hill, *Sol. Phys.* **128**, 321 (1990); D. Haber, J. Toomre, F. Hill, D. Gough, *Astron. Soc. Pac. Conf. Ser.* **76**, 272 (1995); F. Hill, *ibid.*, p. 485. Phase analyses of wave trains are discussed by D. O. Gough, W. J. Merryfield, J. Toomre, *ibid.* **42**, 257 (1993); K. Julien, D. Gough, J. Toomre, *ibid.* **76**, 196 (1995).
 25. D. O. Gough and N. O. Weiss, *Mon. Not. R. Astron. Soc.* **176**, 589 (1976).
 26. These models with coupled compressible convection and radiative transfer use a rectilinear domain with periodic lateral boundaries, permitting flow both through upper and lower bounding surfaces, and employ nonuniform grids in the vertical to yield comparable resolution over each density scale height. Å. Nordlund and R. F. Stein, in *Lect. Notes Phys.* **388**, 141 (1991); M. P. Rast, Å. Nordlund, R. F. Stein, J. Toomre, *Astrophys. J.* **408**, L53 (1993); R. F. Stein and Å. Nordlund, in *Infrared Solar Physics*, D. Rabin, J. Jeffries, C. Lindsey, Eds. (IAU Symposium 154, Kluwer, Dordrecht, Netherlands, 1994), pp. 225–237.
 27. P. Colella and P. R. Woodward, *J. Comp. Phys.* **54**, 174 (1984). Although PPM with monotonicity conditions can deal with sharp-edged structures very well, it involves typically 20 times more operations than the pseudospectral codes used with the viscous Navier-Stokes equations.
 28. These local models have boundary conditions comparable to those of the pseudospectral codes, thus permitting ready intercomparison of results with Navier-Stokes and Euler (PPM) formulations. High-resolution 2D studies of convection with PPM are reported by D. H. Porter and P. R. Woodward, *Astrophys. J. Suppl. Ser.* **93**, 309 (1994), and 3D studies by D. H. Porter, P. R. Woodward, W. Yang, Q. Mei, in *Nonlinear Astrophysical Fluid Dynamics*, R. Buchler and S. T. Gottesman, Eds. (New York Acad. Sci., New York, 1990), pp. 234–258; D. H. Porter, P. R. Woodward, Q. Mei, *Video J. Eng. Res.* **1**, 1 (1991); T. J. Bogdan, F. Cattaneo, A. Malagoli, *Astrophys. J.* **407**, 316 (1993); P. R. Woodward, D. H. Porter, B. K. Edgar, S. E. Anderson, G. Bassett, *Comput. Appl. Math.* **14**, 97 (1995); D. H. Porter and P. R. Woodward, in preparation.
 29. The downflow lanes typically have a mean enstrophy (vorticity squared) at least 10 times larger than regions of upflow. The vorticity is preferentially aligned with the principle direction of strain of the large-scale flow field, which is consistent with vortex stretching being the principle mechanism of enstrophy production.
 30. N. H. Brummell, D. H. Porter, J. Toomre, P. R. Woodward, in preparation.
 31. The interaction between magnetic fields and convection—magnetoconvection—has been studied extensively both analytically and numerically. Reviews on this aspect of solar magnetohydrodynamics are by M. R. E. Proctor and N. O. Weiss, *Rep. Prog. Phys.* **45**, 1317 (1982); D. W. Hughes and M. R. E. Proctor, *Annu. Rev. Fluid Mech.* **20**, 187 (1988); N. O. Weiss, *Geophys. Astrophys. Fluid Dyn.* **62**, 229 (1991); F. Cattaneo, in *Solar Magnetic Fields*, M. Schüssler and W. Schmidt, Eds. (Cambridge Univ. Press, Cambridge, 1993), pp. 261–275. An excellent review of the work on sunspots is by J. H. Thomas and N. O. Weiss, in *Sunspots: Theory and Observations*, J. H. Thomas and N. O. Weiss, Eds. (Kluwer, Dordrecht, Netherlands, 1992), pp. 3–59.
 32. Because of the polarity reversal, the solar magnetic cycle has a 22-year period, or twice that of the activity cycle. Properties of solar magnetic fields are discussed, for example, by E. R. Priest, *Solar Magnetohydrodynamics* (Reidel, Dordrecht, Netherlands, 1982); P. R. Wilson, *Solar and Stellar Activity Cycles* (Cambridge Univ. Press, Cambridge, 1994).
 33. R. J. Defouw, *Astrophys. J.* **209**, 266 (1976); H. C. Spruit, *Astron. Astrophys.* **95**, 155 (1981).
 34. F. Moreno-Insertis, *Astron. Astrophys.* **166**, 291 (1986); A. Ferriz-Mas and M. Schüssler, *Geophys. Astrophys. Fluid Dyn.* **48**, 217 (1989); F. Moreno-Insertis, M. Schüssler, A. Ferriz-Mas, *Astron. Astrophys.* **264**, 686 (1992); P. Calgari, F. Moreno-Insertis, M. Schüssler, *Astrophys. J.* **441**, 886 (1995); F. Moreno-Insertis, P. Calgari, M. Schüssler, *ibid.*, in press.
 35. The mechanism in the solar context was proposed by E. N. Parker [*Astrophys. J.* **122**, 293 (1955)], in the context of the Earth by S. Braginskii [*Sov. Phys. JETP* **20**, 726 (1964); *ibid.*, p. 1462], and on the basis of a two-scale approach by M. Steenbeck, F. Krause, and K.-H. Rädler [*Z. Naturforsch.* **A 21**, 369 (1966)].
 36. Excellent discussions of the α effect are found in H. K. Moffatt, *Magnetic Field Generation in Electrically Conducting Fluids* (Cambridge Univ. Press, Cambridge, 1978); F. Krause and K.-H. Rädler, *Mean-Field Magnetohydrodynamics and Dynamo Theory* (Pergamon, London, 1980); Ya. B. Zel'dovich, A. A. Ruzmaikin, D. D. Sokoloff, *Magnetic Fields in Astrophysics* (Gordon and Breach, New York, 1983).
 37. S. I. Vainshtein and R. Rosner, *Astrophys. J.* **376**, 199 (1991); S. I. Vainshtein and F. Cattaneo, *ibid.* **393**, 165 (1992).
 38. For a review of work on fast dynamos, see A. M. Soward, in *Lectures on Solar and Planetary Dynamics*, M. R. E. Proctor and A. D. Gilbert, Eds. (Cambridge Univ. Press, Cambridge, 1994), pp. 181–217, and references therein.
 39. S. I. Vainshtein and Ya. B. Zel'dovich, *Usp. Fiziol. Nauk* **106**, 431 (1972).
 40. Theoretical discussions and models based on simple flows are found in J. M. Finn and E. Ott, *Phys. Fluids* **31**, 2998 (1988); E. Ott and T. M. Antonsen, *Phys. Rev. A* **39**, 3660 (1989); Y. Du and E. Ott, *Physica D* **67**, 387 (1993); *J. Fluid Mech.* **257**, 265 (1993). More computational examples are found in A. D. Gilbert and S. Childress, *Phys. Rev. Lett.* **65**, 2133 (1990); D. J. Galloway and M. R. E. Proctor, *Nature* **356**, 691 (1992).
 41. F. Cattaneo, E. Kim, M. R. E. Proctor, L. Tao, *Phys. Rev. Lett.*, in press.
 42. A. V. Grunin and P. H. Diamond, *ibid.* **72**, 1651 (1994).
 43. Fully nonlinear simulations of dynamo action have recently been discussed by M. Meneguzzi and A. Pouquet, *J. Fluid Mech.* **205**, 297 (1989); A. Brandenburg *et al.*, *Astron. Astrophys.* **232**, 277 (1990);

- L. Tao, F. Cattaneo, S. I. Vainshtein, in *Solar and Planetary Dynamos*, M. R. E. Proctor, P. C. Matthews, A. M. Rucklidge, Eds. (Cambridge Univ. Press, Cambridge, 1993), pp. 303-310.
44. J. Christensen-Dalsgaard, J. Schou, M. J. Thompson, J. Toomre, *Astron. Soc. Pac. Conf. Ser.* **76**, 212 (1995); in preparation.
45. Extensive examples of images with SXT are in C. C. Peterson, M. Bruner, L. Acton, Y. Ogawara, *Sky Telesc.* **86**, 20 (September 1993); see also S. Tsuneta *et al.*, *Sol. Phys.* **136**, 37 (1991); T. Shimizu *et al.*, *Astrophys. J.* **422**, 906 (1994).
46. Data obtained with TRC are described by B. Foing and R. M. Bonnet, *Astron. Astrophys.* **136**, 133 (1984).
47. High-resolution imaging with Swedish Solar Observatory on La Palma and the data reduction are described by R. A. Shine *et al.* [*Astrophys. J.* **430**, 413 (1994)], and CH-bandhead studies are described by T. E. Berger *et al.* (in preparation).
48. The ratio of the inner to outer boundary of the shell is 0.68, across which the density changes by factor $\chi = 10$. Here $Ra = 3 \times 10^7$, $Ta = 10^9$, $Pr = 0.05$, $Ro \sim 0.8$, and $Re \sim 5 \times 10^4$. The spatial resolution is 129 in radius, 320 in latitude, and 80 in a 45° longitude slice (l up to 213).
49. The f -plane compressible simulation with 256^2 by 130 spatial modes in a domain $4 \times 4 \times 1$ involves $Ra = 10^7$, $Ta = 2 \times 10^7$, $Pr = 0.1$, $\chi = 10$, $\phi = 45^\circ$, and $Ro = 2.2$, with Reynolds numbers $Re \sim 2000$ and $Re_\lambda \sim 12$.
50. The simulation with 96^2 by 64 spatial modes involves $Ra = 5 \times 10^5$, $Ta = 10^7$, $Pr = 0.1$, $\chi = 10$, $\phi = 45^\circ$, and $Ro = 0.7$, with Reynolds numbers $Re \sim 1000$ and $Re_\lambda \sim 10$.
51. The PPM simulation of nonrotating convection was carried out with 512^2 by 256 spatial zones in a domain $2 \times 2 \times 1$, involving $Ra \sim 3 \times 10^{12}$, $Pr \sim 10^{-4}$, and $\chi = 10$, with Reynolds number $Re \sim 3 \times 10^7$.
52. This work was supported in part by the National Aero-

nautics and Space Administration through the Space Physics Theory Program grants NAG5-2256 and NAG5-1485 and the HPCC team grant NAG5-2218, and by the National Science Foundation through the Grand Challenge Applications Group grant ECS-9217394. Computations were performed at the Pittsburgh Supercomputing Center on the Cray C-90 and Cray T3D and at the Cornell Theory Center on the IBM SP-2 under MetaCenter grant MCA93S005P. We thank P.-Ø. Hvidsten and Ø. Andreassen of the Norwegian Defence Research Establishment, and the original developers at the University of Minnesota, for use of the Brick-of-Bytes volume-rendering software. We acknowledge T. Clune, G. Glatzmaier, D. Gough, H. Goldstein, D. Hughes, N. Hurlburt, F. Moreno-Inertis, Å. Nordlund, D. Porter, M. Rast, M. Schüssler, R. Stein, A. Title, J. Thomas, P. Woodward, and E. Zweibel for helpful advice and assistance in the preparation of this article.

Modeling Ocean Circulation

Albert J. Semtner

Ocean numerical models have become quite realistic over the past several years as a result of improved methods, faster computers, and global data sets. Models now treat basin-scale to global domains while retaining the fine spatial scales that are important for modeling the transport of heat, salt, and other properties over vast distances. Simulations are reproducing observed satellite results on the energetics of strong currents and are properly showing diverse aspects of thermodynamic and dynamic ocean responses ranging from deep-water production to El Niño. Now models can represent not only currents but also the consequences for climate, biology, and geochemistry over time spans of months to decades. However, much remains to be understood from models about ocean circulation on longer time scales, including the evolution of the dominant water masses, the predictability of climate, and the ocean's influence on global change.

chemical tracers have local maxima in the cores of strong currents. Consequently, a proper representation of transports of these properties involves not only the means of individual variables but also relatively small-scale correlations with velocity. Furthermore, significant changes of the currents and property transports occur in response to modified surface forcing, and the correct simulation of these responses is crucial to solving a variety of problems ranging from understanding the history of the Earth system to predicting future climates. These are the challenges for ocean modeling.

An early paradigm. A first significant modeling effort extended over the decade of the 1960s at the Geophysical Fluid Dynamics Laboratory (GFDL) (now located at Princeton University and operated by the National Oceanic and Atmospheric Administration). Bryan built an ocean model that was to be used with atmospheric models to study climate. In rapid succession, he and co-worker Cox developed a 2D model, a 3D box model, and then a model of full circulation, with variable density as well, for the world ocean with its complex coastline and bottom topography (6).

The models used space-centered explicit finite differencing, and the last version used a variable number of vertical levels to represent the complex geometry. All of the models used an assumption known as the "rigid lid" approximation to eliminate high-speed external gravity waves and allow a longer time step: the upper surface was held fixed but could support pressure changes related to waves of lower speed and currents of interest. As a result, ocean tides and other waves having the speed of tsunamis were filtered out. Use of the rigid lid created an ancillary 2D equation at every time step to obtain the vertically averaged component of the currents. Bryan's 1969 model used partial differential equations, formulated in rotating spherical coordinates, for horizontal velocity, temperature, and salinity, plus hydrostatic balance, incompressibility, and an empirical equation for density. Processes occurring on scales smaller than the

The ocean is now well known to play a dominant role in the climate system because it can initiate and amplify climate change on many different time scales. The best known examples are the interannual variability of El Niño (1) and the potential modification of the major patterns for oceanic heat transport as a result of increasing greenhouse gases (2). Yet the ocean has been very much undermeasured for most of the history of ocean science. Even though systematic observations began in the 1880s with pioneering observations by Nansen and others (3), the seagoing and theoretical efforts were mainly oriented toward describing large-scale circulation (4), which was often regarded as steady for lack of more detailed information. It was not until the 1960s, when long-distance tracking of drifting buoys at mid-depth showed currents to be highly variable on quite small spatial scales (5), that oceanographers became aware of the immensity of their task.

In dealing with an undersampled natural fluid system, it is extremely helpful to invoke the simulation capability of supercomputers to improve understanding of basic processes and

their interconnectedness, as well as to help interpret sparse observations. This article describes the development of ocean modeling as it has been influenced by improved methods, more powerful computers, and data from the latest measuring systems. Recent successes that pave the way to better physical understanding and more reliable ocean prediction are emphasized, although issues of running coupled atmosphere-ocean models are not discussed. Some remaining problems are highlighted briefly.

The Evolution of Models

The ocean is a turbulent fluid that is driven mainly by the mechanical forcing of the winds and the net effect on density of surface exchanges of heat and moisture. It responds according to physical laws for the conservation of mass, momentum, energy, and other properties. The resulting three-dimensional (3D) flows are strongly influenced by Earth's rotation and are regulated by internal mixing and boundary friction. The currents are particularly narrow and strong at the western side of ocean basins and in a belt around Antarctica. Many ocean properties such as temperature, salinity, dissolved oxygen, and biogeo-

The author is in the Department of Oceanography, Naval Postgraduate School, Monterey, CA 93943, USA.